



Since January 2020 Elsevier has created a COVID-19 resource centre with free information in English and Mandarin on the novel coronavirus COVID-19. The COVID-19 resource centre is hosted on Elsevier Connect, the company's public news and information website.

Elsevier hereby grants permission to make all its COVID-19-related research that is available on the COVID-19 resource centre - including this research content - immediately available in PubMed Central and other publicly funded repositories, such as the WHO COVID database with rights for unrestricted research re-use and analyses in any form or by any means with acknowledgement of the original source. These permissions are granted for free by Elsevier for as long as the COVID-19 resource centre remains active.



# Facilitating SARS CoV-2 RNA-Dependent RNA polymerase (RdRp) drug discovery by the aid of HCV NS5B palm subdomain binders: In silico approaches and benchmarking

Laila K. Elghoneimy<sup>a</sup>, Muhammad I. Ismail<sup>b</sup>, Frank M. Boeckler<sup>c</sup>, Hassan M.E. Azzazy<sup>a</sup>, Tamer M. Ibrahim<sup>d,\*</sup>

<sup>a</sup> Department of Chemistry, School of Sciences and Engineering, American University in Cairo, AUC Avenue, SSE # 1184, P.O. Box 74, New Cairo, 11835, Egypt

<sup>b</sup> Department of Pharmaceutical Chemistry, Faculty of Pharmacy, The British University in Egypt, Al-Sherouk City, Cairo-Suez Desert Road, 11837, Cairo, Egypt

<sup>c</sup> Department of Pharmacy, Eberhard-Karls University, Auf der Morgenstelle 8, 72076, Tuebingen, Germany

<sup>d</sup> Department of Pharmaceutical Chemistry, Faculty of Pharmacy, Kafrelsheikh University, Kafrelsheikh, 33516, Egypt

## ARTICLE INFO

### Keywords:

COVID-19  
Nsp12  
NS5b  
Docking  
VS  
Benchmarking  
DEKOIS 2.0

## ABSTRACT

Corona Virus 2019 Disease (COVID-19) is a rapidly emerging pandemic caused by a newly discovered beta coronavirus, called Severe Acute Respiratory Syndrome Coronavirus 2 (SARS CoV-2). SARS CoV-2 is an enveloped, single stranded RNA virus that depends on RNA-dependent RNA polymerase (RdRp) to replicate. Therefore, SARS CoV-2 RdRp is considered as a promising target to cease virus replication. SARS CoV-2 polymerase shows high structural similarity to Hepatitis C Virus-1b genotype (HCV-1b) polymerase.

Arising from the high similarity between SARS CoV-2 RdRp and HCV NS5B, we utilized the reported small-molecule binders to the palm subdomain of HCV NS5B (genotype 1b) to generate a high-quality DEKOIS 2.0 benchmark set and conducted a benchmarking analysis against HCV NS5B. The three highly cited and publicly available docking tools AutoDock Vina, FRED and PLANTS were benchmarked. Based on the benchmarking results and analysis via pROC-Chemotype plot, PLANTS showed the best screening performance and can recognize potent binders at the early enrichment. Accordingly, we used PLANTS in a prospective virtual screening to repurpose both the FDA-approved drugs (DrugBank) and the HCV-NS5B palm subdomain binders (BindingDB) for SARS CoV-2 RdRp palm subdomain. Further assessment by molecular dynamics simulations for 50 ns recommended diosmin (from DrugBank) and compound 3 (from BindingDB) to be the best potential binders to SARS CoV-2 RdRp palm subdomain. The best predicted compounds are recommended to be biologically investigated against COVID-19. In conclusion, this work provides *in-silico* analysis to propose possible SARS CoV-2 RdRp palm subdomain binders recommended as a remedy for COVID-19. Up-to-our knowledge, this study is the first to propose binders at the palm subdomain of SARS CoV2 RdRp. Furthermore, this study delivers an example of how to make use of a high quality custom-made DEKOIS 2.0 benchmark set as a procedure to elevate the virtual screening success rate against a vital target of the rapidly emerging pandemic.

## 1. Introduction

A pandemic coronavirus had arisen at the end of 2019 resulting in a worldwide crisis. This novel coronavirus is known as Severe Acute Respiratory Syndrome Coronavirus 2 (SARS CoV-2) that causes a pulmonary disease with pneumonia-like symptoms called Corona Virus 2019 Disease (COVID-19). On the November 14, 2020, the World Health Organization (WHO) Coronavirus Disease (COVID-19) Dashboard reported that there have been 53,164,803 confirmed cases of COVID-19,

including 1,300,576 deaths, worldwide. This raises the attention to essentially develop a valid cure for this global pandemic. Coronaviruses (CoVs) are positive sense, single stranded RNA viruses that belong to *Coronaviridae* family (order *Nidovirales*, family *Coronaviridae*, and sub-family *Orthocoronavirinae*) [1,2]. The *Coronaviridae* family is further classified to alpha, beta, gamma and delta genera [1,2]. SARS CoV-2 is the new beta human coronavirus [3–5].

The SARS CoV-2 viral genome is around 30 kb in length encoding to 14 open reading frames (ORFs) at the N-terminal and 4 structural

\* Corresponding author.

E-mail addresses: [Tamer\\_Mohamad@pharm.kfs.edu.eg](mailto:Tamer_Mohamad@pharm.kfs.edu.eg), [tamer.ibrahim2@gmail.com](mailto:tamer.ibrahim2@gmail.com) (T.M. Ibrahim).

<https://doi.org/10.1016/j.complbiomed.2021.104468>

Received 7 February 2021; Received in revised form 25 April 2021; Accepted 30 April 2021

Available online 11 May 2021

0010-4825/© 2021 Elsevier Ltd. All rights reserved.

proteins at the C-terminal [6–9]. The open reading frames, ORF 1a and ORF 1b encode two polyproteins (pp. 1a and pp. 1 ab) [8,9]. These precursor polyproteins will be cleaved into 16 non-structural proteins (nsp), which are essential for viral replication as well as the host immunity replication [6–9]. SARS CoV-2 RdRp, or nsp12, is the enzyme responsible for CoV-2 replication by catalyzing the synthesis of RNA from RNA template [6,10]. Nsp12 is not active on its own, it needs the assistance of two accessory units nsp7 and nsp8 [6,7,10,11]. The nsp12 is composed of a canonical capped right-handed RdRp domain (S367–F920) at the C-terminal, a nidovirus specific N-terminal extension domain (D60–R249) that adopts a nidovirus RdRp-associated nucleotidyltransferase (NiRAN) and an interface (A250–R365) linking the previous two domains together [6]. Additionally, CoV-2 RdRp is uniquely characterized by a  $\beta$ -hairpin (D29–K50) at the N-terminus [6]. The RdRp domain is consisted of three conserved subdomains; finger (L366 to A581 and K621 to G679), palm (T582 to P620 and T680 to Q815) and thumb (H816 to E920), which further contains seven invariant motifs (A to G) [6]. Motifs A to E are located in the palm, while F (L544 to V557) and G (D499 to L514) motifs are in the finger subdomain [6]. Motif A (611-TPHLMGWDYPKCDRAM-626) and Motif C (753-FSMMLSDDAVVCFN-767) form the active site of the nsp12 by containing the classical catalytic residues that are essential for the divalent cation binding. These residues are D618 in A motif and (759–SDD-761) in C motif [6]. Interestingly, based on a structural comparison study, these catalytic residues are invariant among most viral polymerases, such as (D220) and (317–GDD-319) in hepatitis C virus (HCV) NS5B [6].

An alignment study of a huge data set of RdRps, including nsp12, shows the extreme similarity between the secondary structure of the polymerases, from different RNA viruses, especially at the catalytic binding domains [5]. According to the previous study, the top three similar viruses to SARS CoV-2 are poliovirus type 1, HCV genotype 2a, and HCV genotype 1b [5]. Due to the lack of poliovirus inhibitors and the limited NS5B-2a non-nucleoside inhibitors, HCV NS5B-1b inhibitors were chosen to generate DEKOIS 2.0 benchmark set and conduct a benchmarking analysis.

Structure based virtual screening (SBVS) is a computational technique that is widely used during the early stages of drug discovery. It is based on the molecular docking of a novel group of bioactive compounds against the binding site of the 3D structure of the target protein. It aims at predicting the binding poses of the new candidates and understanding the structural aspects of the targets binding sites. Compounds that show high predicted binding scores will be selected for further biological investigations [12–15]. To guarantee more successful VS efforts, the docking tool needs to be assessed by the aid of benchmarking molecular sets [16,17].

The objective of the present study is to provide basis on how to repurpose FDA-approved drugs (from DrugBank database) and HCV-NS5B (1b genotype) palm inhibitors (from BindingDB repository) against the palm pocket of SARS CoV-2 RdRp. Up-to-our knowledge, this study is the first to propose binders at the palm subdomain of SARS CoV2 RdRp. Based on the high similarity between the both polymerases of HCV-1b and SARS CoV-2, we hypothesized that a benchmarking investigation against the HCV-NS5B palm subdomain will be useful in recommending a docking workflow for targeting the palm subdomain of SARS CoV-2, especially due to the lack of known binders for the later. For this, we carried out benchmarking analysis for the highly cited and publicly available docking tools, AutoDock Vina, PLANTS and FRED.

## 2. Results and discussions

### 2.1. Selection of HCV-NS5B actives for decoys generation

The active set to be used in the decoy generation for benchmarking study needs to include a high variety of chemotypes with potent reported activity. As mentioned earlier, polymerase sites for inhibition are

either the active site or the allosteric sites in thumb and palm subdomains [18]. The active site is targeted by nucleotide inhibitors that act as alternative substrates for polymerases [18]. Upon the incorporation of such inhibitors into the growing RNA chain, elongation step will be terminated. Since they are nucleotide analogues, they are very limited in terms of diversity. Modifications are only concerned with Ribose sugar substitutions and/or modifications at the base part [18]. On the contrary, non-nucleoside inhibitors possess highly diverse scaffolds that inhibit polymerases through blocking the nucleotide entry, hence, interfere with the RNA initiation and elongation steps [18]. Here we selected our active set to be composed of NS5B-1b allosteric palm inhibitors based on the following justifications: the palm site is the most conservative subdomain with 15 Å in width and 20 Å in depth [18]. Consequently, a wide range of inhibitors targeting palm subdomain is available which will enrich the active set. Additionally, this subdomain encompasses the active site so targeting it will lead to blocking the nucleotide entry, hence, interfering with the RNA initiation and elongation steps [18]. Moreover, literature is mainly focusing on nucleotide analogues and lacks investigation about palm subdomain especially for the COVID-19.

The palm allosteric pocket is known to be the interface between palm and thumb subdomains. In addition, palm residues from 363 to 369 are forming a deep hydrophobic pocket called primer grip. The primer grip region is formed from one wall of the palm and the opposite wall of a  $\beta$ -hairpin loop from the thumb [18]. This justifies why palm inhibitors may go through interactions with residues from the thumb site like Tyr448 (Fig. 1).

To build our active set (Table S1 in the Supplementary Material), we downloaded around 2800 compounds from BindingDB database acting on HCV polymerase (NS5B). Of these compounds, 233 specifically inhibit 1b genotype, and 140 target the palm subdomain. In addition to the compounds reported in BindingDB [19], we manually compiled scaffolds from literature [18] to achieve the best diversity in the chemotypes. As representatives for each scaffold, we selected two to four molecules, with the lowest IC<sub>50</sub> values. The activity is ranging from IC<sub>50</sub> values from 5 nM to 470 nM. It is important to mention that irreversible inhibitors were excluded from the set. Collectively, these compounds represent the following scaffold classes: Benzothiadiazine, benzothiazine, 1,1-dioxoisothiazole, 5,6-dihydro-1H-pyridin-2-one, proline sulfonamide, acrylic acid, N-acyl pyrrolidine, benzamide, nicotinamide, anthranilic acid, benzodiazepine, sulphone and benzofuran [18,20–32].

### 2.2. Selection of representative PDB structure(s) for HCV NS5B-1b

For selecting a protein structure for the benchmarking study, we downloaded the NS5B structures from the PDB (Table S2 in SM). A special focus was dedicated for protein structures co-crystallized with a ligand in the palm subdomain to consider any structural changes that may happen during ligand-protein binding event, and for PDB structures of the genotype 1b. Based on the superposition of five of these high-resolution structures, we did not observe a significant difference in their backbone or side chain conformations as indicated by the low values of their pairwise RMSD (Fig. S1 in SM). Accordingly, we selected the HCV-NS5B (PDB ID: 3HHK) to be used for the benchmarking study.

### 2.3. Benchmarking

There are certain requirements for providing meaningful molecular benchmarking sets for structure-based VS. First, a well curated and characterized set of ligands, also often referred to as actives, must be compiled. Second, decoy structures must be selected based on the high-quality criteria (e.g., DEKOIS 2.0 protocol [33–35]). And finally, a well-suited 3D structure is needed to model the ligand binding site. These essential requirements confine the eligible targets for benchmark set generation.

Generally, benchmarking performance is a target dependent.

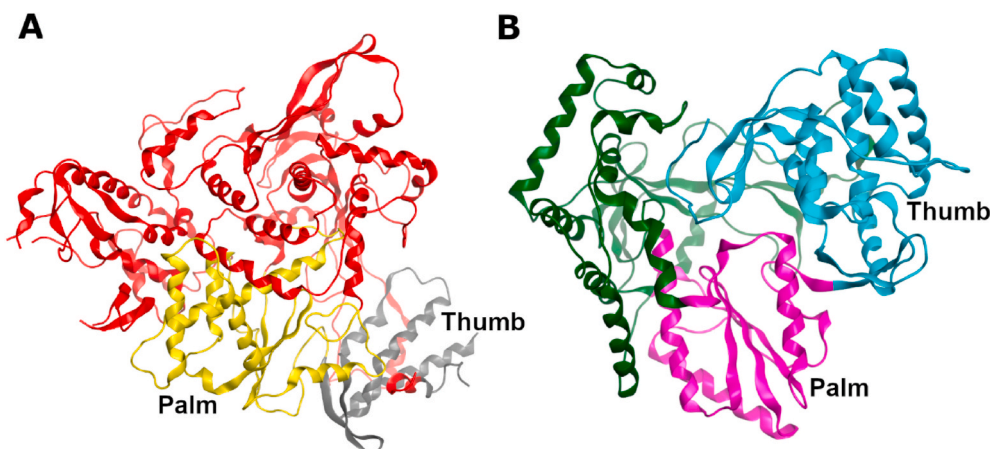


**Fig. 1.** 3D representation of SARS-CoV-2 RdRp (PDB ID: 7BV1) and HCV-1b NS5B (PDB ID: 3HHK): A is the ribbon diagram of RdRp in red. The yellow part is the palm, while the grey part is the thumb subdomain. B is the NS5B in green. The cyan part is the thumb and the purple region is for the palm site.

However, highly similar, and conserved binding sites usually show comparable performances by a docking tool. For instance, GLIDE appeared to be the best performing docking tool in recognizing the active molecules in a pool of their decoys indicated by the best pROC-AUC value, compared to other docking tools for the closely related kinases in a reported study [16]. Likewise, AutoDock Vina appeared to be the best performing docking tool for the closely related COX-1 and COX-2 enzymes. Inspired by these observations, and due to the lack of known binders to palm subdomain of SARS-CoV-2 RdRp, we compiled an active set for its closely related target, HCV-NS5B (palm subdomain). We evaluated the screening performance of some publicly available and highly cited docking programs FRED, AutoDock Vina and PLANTS against HCV-NS5B (palm subdomain). The outcome of this benchmarking efforts is certainly useful to gain insights and decide which docking tool can be used for VS campaigns against the closely related SARS-CoV-2 RdRp palm subdomain.

The benchmarking against the HCV-NS5B (palm subdomain) showed that PLANTS is the best performing tool for both cases when excluding and including the key water molecules in the proximity of the co-crystal ligand, as shown in Fig. 2. The screening performance indicated by pROC-AUC values are 0.97, 0.66 and 0.36 for PLANTS, AutoDock Vina and FRED, respectively, when including the key water molecules (Fig. 2A). Also, the pROC-AUC values are 0.81, 0.47 and 0.34 for

PLANTS, AutoDock Vina and FRED when excluding the key water molecules (Fig. 2B). Unlike FRED, PLANTS and AutoDock Vina docking tools exhibited better-than-random performance, i.e., pROC-AUC value > 0.43, in both cases.

We examined the scaffold clusters enrichment with the “pROC-Chemotype” [36,37] plot (see Fig. 3) for the benchmarking of HCV-NS5B (palm subdomain) using PLANTS docking tool. The diversity of the established chemotypes (13 scaffolds) highlights the challenging nature of the benchmarking against the employed docking tools. The bioactivity data of the active set are symbolized by *level of activity* (LOA), extending from  $10^{-7}$  to  $10^{-9}$  M, and reported as *type of data* (TOD), as seen in Fig. 3A. The pROC-Chemotype plot visualized that PLANTS is able to enrich high affinity binders at early enrichment (Fig. 3A). Elucidating the docking poses of the best scored actives underlines that they reproduced the key interactions of the co-crystal ligand in the palm subdomain, as shown in Fig. 3. Moreover, at 1% of the score-ordered library, only two decoys were enriched, and many bioactive molecules were recognized, leading to an Enrichment Factor (EF 1%) of 20.0. Interestingly, this indicates a promising predictive power of PLANTS since it can recognize active molecules 20 times more than the random performance at early enrichment (e.g., library cutoff 1%). This encourages us to employ PLANTS in prospective VS against the closely related SARS-CoV-2 RdRp (palm subdomain).

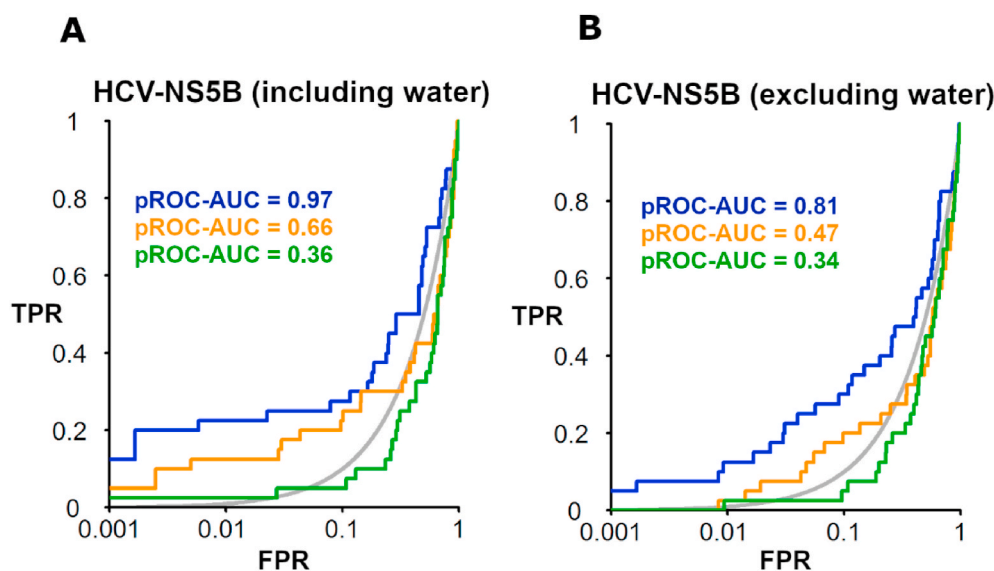


**Fig. 2.** pROC plots of benchmarking experiments against HCV-NS5B (palm subdomain - PDB ID: 3HHK) when including and excluding key water molecules in the palm binding site for (A) and (B), respectively. The curves of PLANTS, AutoDock Vina and FRED are presented by blue, orange, and green lines, respectively. The random screening performance is shown as a grey line. The Y-axis is the true positive rate (TPR), which reflects the fraction of detected bioactives. While the X-axis shows the decoys retrieved fraction that is known as false positive rate (FPR).





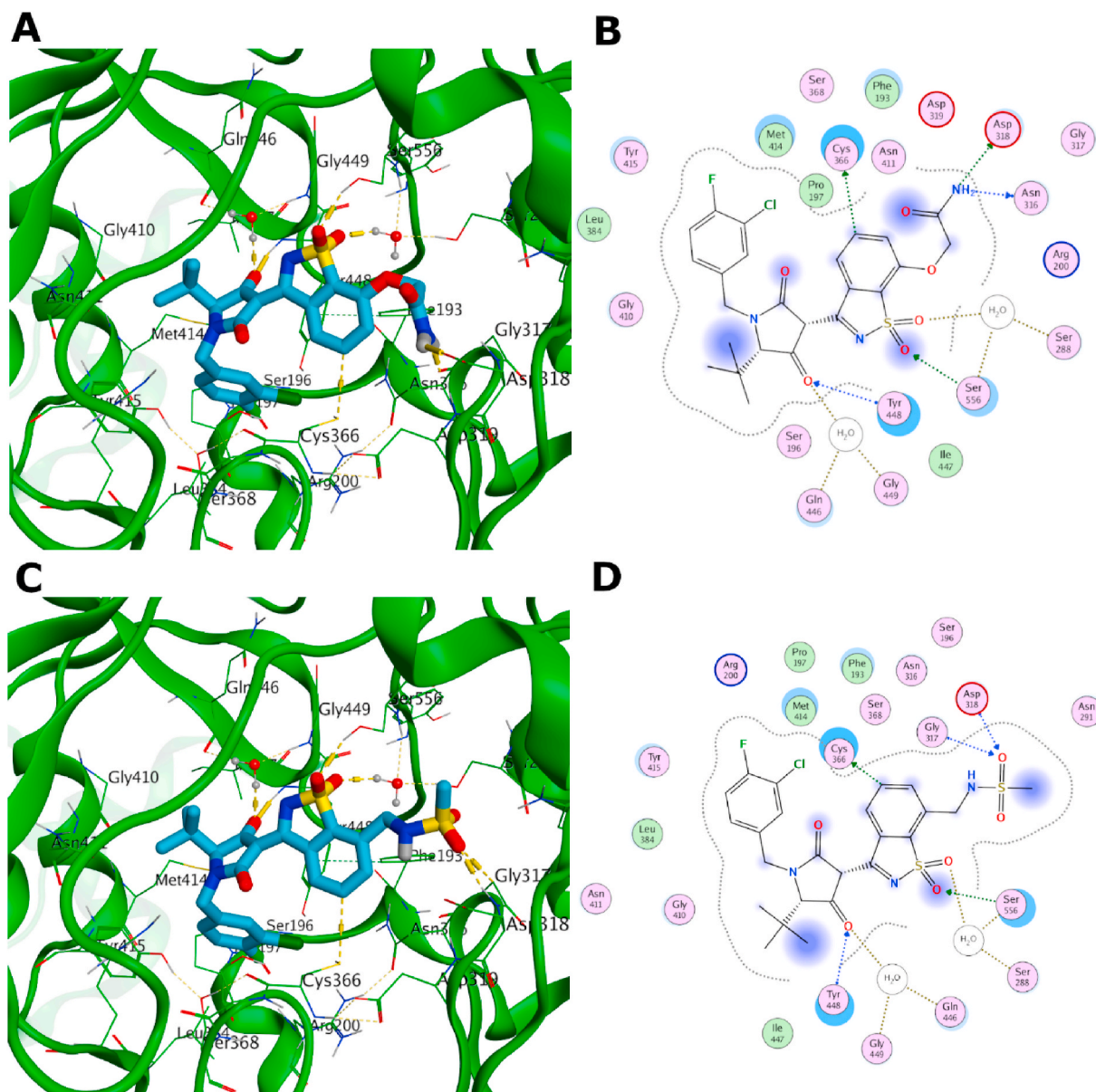


**Fig. 4.** Docking poses of the best two ranked compounds (docking rank 1 and 2) from the active set in the palm subdomain of HCV-NS5B-1b (PDB ID: 3HHK), for (A, B) and (C, D), respectively. Dashed lines indicate favorable interactions. Non-polar hydrogens are omitted for clarification.

palm subdomain to consider the conformational changes upon ligand binding. We did not observe significant changes in the palm backbone and side chains between the apo and the complexed structures with nucleotide inhibitors in the active site (data not shown). Accordingly, we selected the apo structure (PDB ID: 7BV1) for the prospective VS on the palm subdomain. This would block the nucleotide entry, and therefore, disturb the RNA initiation and elongation steps for the virus replication.

The VS outcome of the best 1% of the score-ordered list of the DrugBank database and HCV-NS5B inhibitors of BindingDB are shown in Table 1 and Table 2, respectively. Analyzing the binding poses of all molecules, we noticed that they mainly occupy one of the four sites shown in (Fig. 5). Inspired by HCV-NS5B palm inhibitors, it emerged that the inhibition occurs when the inhibitor resides in the palm pocket in front of the F motif (region d for SARS CoV2 RdRp) in the finger subdomain (Fig. S2 in SM). The F motif is responsible for directing the incoming NTPs into the active site. Consequently, the entry path to the active site will be blocked, leading to the inhibition of initiation and elongation steps during the viral replication [6]. Accordingly, we

dedicate focus on molecules that reside at site d of the RdRp palm subdomain from the best ranked 1%, as illustrated in Fig. 6 and Fig. 7.

The five top scored compounds that showed better localization of the palm pocket were chosen to elucidate their poses and binding interactions. Starting with the DrugBank results, Quinupristin, Acetyldigitoxin, Diosmin, Hesperidin and Voxilaprevir are the ones that met the previous criteria.

Fig. 6 illustrates the docking pose of Quinupristin in the palm pocket of SARS-CoV-2 RdRp (PDB ID: 7BV1). Quinupristin is an anti-bacterial agent that is used mainly in combination with Dalfopristin to treat bacterial infections. It binds near the 50S ribosomal subunit, therefore inhibits the late phase of protein synthesis [38]. Its postulated binding pose in the RdRp (Fig. 6) exhibited hydrogen bonding interactions with the side chains of Asp865, Gl590 and Asn496.

Acetyldigitoxin is a cardioactive derivative of digitoxin that is used in different types of arrhythmia and congestive heart failure [39]. Its docking pose (Fig. S3 in SM) reveals H-bond interactions with Ala685, Lys577 and Asn496 residues. Diosmin and Hesperidin are bioflavonoids, found in some plants, such as citrus fruits. Diosmin is available as

**Table 1**

The best ranked 1% of the VS efforts for FDA-approved drugs against the SARS CoV-2 RdRp Apo form (PDB ID: 7BV1).

Docking rank	Drug	Docking score	Mwt	DrugBank ID	Status
1	Bromperidol	-96.03	420.3	DB12401	approved; investigational
2	Haloperidol	-95.18	375.9	DB00502	Approved
3	Bisoctrizole	-94.74	658.9	DB11262	Approved
4	Quinupristin	-93.99	1022.2	DB01369	Approved
5	Panobinostat	-93.31	349.4	DB06603	approved; investigational
6	Ceforanide	-91.87	519.6	DB00923	Approved
7	Acetyldigitoxin	-91.87	806.9	DB00511	Approved
8	Diosmin	-91.55	608.5	DB08995	approved; investigational
9	Hesperidin	-91.44	610.6	DB04703	approved; investigational
10	Voxilaprevir	-91.39	868.9	DB12026	approved; investigational
11	Nandrolone decanoate	-91.31	428.6	DB08804	approved; illicit
12	Delamanid	-90.85	534.5	DB11637	approved; investigational
13	Hexafluronium	-90.75	502.7	DB00941	Approved
14	Vilazodone	-90.41	441.5	DB06684	Approved
15	Ticagrelor	-89.17	522.6	DB08816	Approved
16	Flibanserin	-88.88	390.4	DB04908	approved; investigational
17	Quinapril	-88.71	438.5	DB00881	approved; investigational
18	Digoxin	-88.44	780.9	DB00390	Approved
19	Lymecycline	-88.41	602.6	DB00256	approved; investigational
20	Antrafenine	-88.25	588.5	DB01419	Approved
21	Fosaprepitant	-88.23	614.4	DB06717	Approved

nutritional supplements in the United States. Both Diosmin and Hesperidin are used in the treatment of several venous diseases, like hemorrhoids, varicose veins, and venous stasis [40]. Diosmin docking pose appeared to participate in several H-bonds with Ser682, Asp684, Asp760, Gly590 and Ala688 (Fig. S4 in SM). While Hesperidin docking pose displayed H-bond interactions with Ser592, Val588 and Gly590 residues (Fig. S5 in SM). Interestingly, Voxilaprevir is a NS3/4A serine protease HCV inhibitor that is used against hepatitis C virus, especially with genotype 1 [41]. Its docking pose shows H-bond interactions with Ala685, Asn496, Thr687 and Ala688, as shown in Fig. S6 (SM).

Regarding the VS of HCV-NS5B inhibitors from BindingDB database [19], compounds numbers 1, 2, 3, 4 and 5 exhibited the best localization of the palm pocket (PDB ID: 7BV1) by occupying site d effectively. Compounds 1, 3 and 5 contain benzothiadiazine scaffold, whereas compounds 2 and 4 possess benzimidazole ring system. The docking pose of compound 1 exhibited in Fig. 7, while the docking poses 2, 3, 4 and 5 are displayed in Fig. S7, S8, S9 and S10 in SM, respectively. Compounds number 1 and 3 show H-bond interactions with Gly590 via the benzothiadiazine ring, and another H-bond interaction with Lys577 via the carbonyl oxygen of the terminal amide group. However, Lys577 displays H-bond interaction with the carbonyl oxygen of the carboxylic group of compound number 2. Uniquely, compound 4, possessing an indole ring, facilitates two interactions; one with Ala685 as a H-bond donor, and the other one is a pi interaction between the pyrrole ring and Tyr689 residue.

## 2.5. Molecular dynamics simulations

The three top-enriched ligands in both BindingDB and DrugBank databases were subjected to 50 ns molecular dynamics (MD) simulations for testing the docked-pose time-stability in the binding sites. An additional run was conducted for the apo protein to account for its dynamics as a reference, resulting in a total of 7 MD runs. Analysis of radius of gyration (rgyr), root mean square deviation (RMSD), and root mean square fluctuation (RMSF) for the protein are shown in Fig. 8. Radius of gyration is a measure of protein structure compactness during the simulation time. As shown in Fig. 8, there is no great fluctuation in the rgyr of the 6 protein complexes compared to the apo structure. This gives an indication of the low conformational changes of the protein throughout the simulation, and hence, its stability [53]. RMSD is a measure of protein stability during the simulation time. RMSD is measured for the alpha carbon atoms. RMSD of the 6 protein complexes are comparable to that of the apo protein which means the stability of

the protein structure during the simulations. Per residue RMSF measures the conformational changes that happen to each protein residue. The terminal amino acids show the highest RMSF reflected by the high free movement of their free loops. However, the binding site amino acids show low RMSF (<2 Å) indicating the relative strong binding of the complexed ligands and minimal conformational changes in these residues.

Analysis of ligand RMSD of heavy atoms and hydrogen bonds of ligands in the binding site are shown in Fig. 9. RMSD measurements show diosmin to have the least RMSD indicating its highest stability inside the binding site. Compound 3 also showed RMSD comparable to that of diosmin indicating its relative strong binding. Both compounds showed low fluctuation in their RMSD throughout the simulation time. The dynamics of these complexes converged after 10 ns of simulation, implying the idea that the structural changes present in these complexes with RdRp (palm subdomain) converged to a stable structure. On the other hand, compound 1 showed the highest RMSD indicating its highest deviation from its original docked pose. It also shows high fluctuation in its RMSD indicating its instability of the binding pose throughout the simulation time.

Concerning the number of hydrogen bonds formed between each ligand and its respective protein (Fig. 9), diosmin showed the highest number of hydrogen bonds indicating its strong binding relative to other ligands, followed by compound 3 which showed the second-highest hydrogen bonds formed with the protein showing its relatively strong binding. Quinupristin comes in third place followed by the other three ligands, acetyldigitoxin, compound 1, and compound 2.

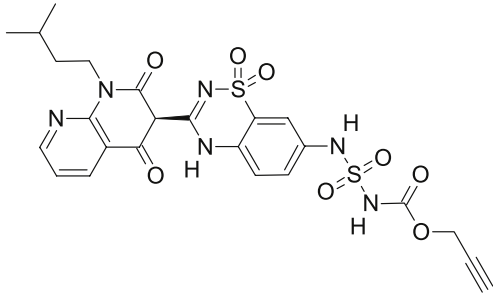
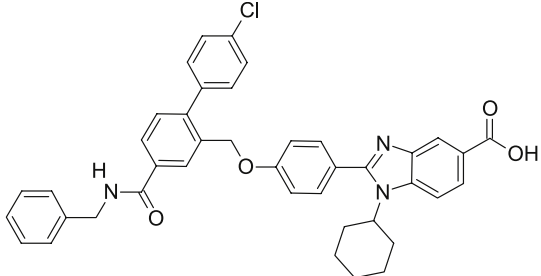
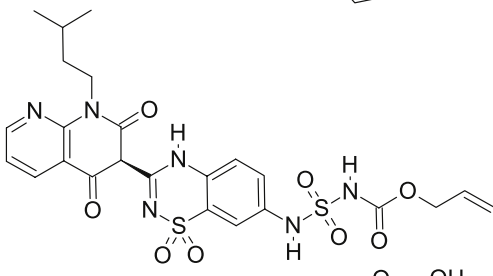
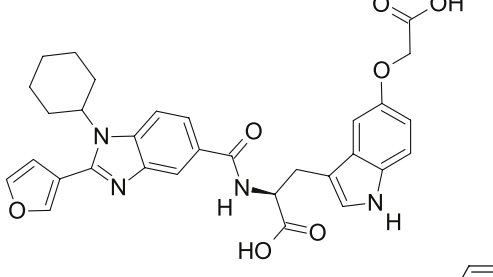
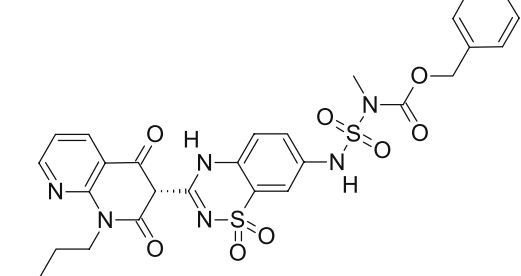
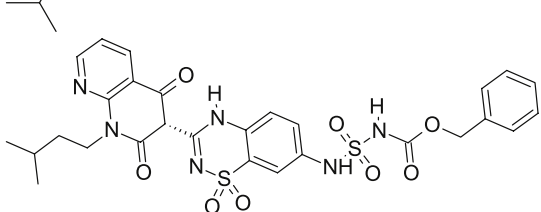
Generally, the results of RMSD and hydrogen bonds analysis show diosmin to have the best binding in the DrugBank series and compound 3 in the BindingDB series.

## 3. Conclusion

To conclude, we relied on the high similarity between SARS CoV-2 RdRp and HCV-NS5B (genotype 1b) to compile a diverse active set from the reported HCV-NS5B palm inhibitors from both the BindingDB repository and literature. The highly diverse active set contains 13 different scaffolds, namely: Benzothiadiazine, benzothiazine, 1,1-dioxo-isothiazole, 5,6-dihydro-1H-pyridin-2-one, proline sulfonamide, acrylic acid, N-acyl pyrrolidine, benzamide, nicotinamide, anthranilic acid, benzodiazepine, sulphone and benzofuran. Consequently, we generated high-quality decoy set using DEKOIS 2.0 protocol and performed benchmarking against HCV-NS5B-1b palm subdomain (PDB ID:

**Table 2**

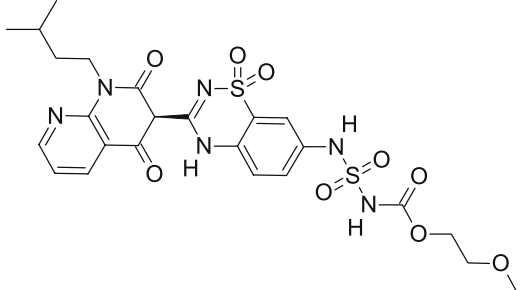
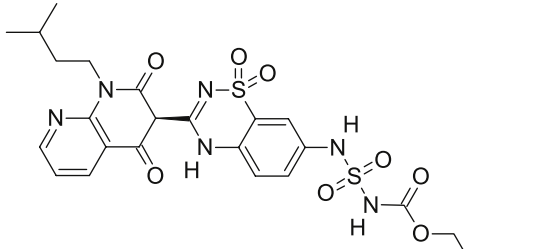
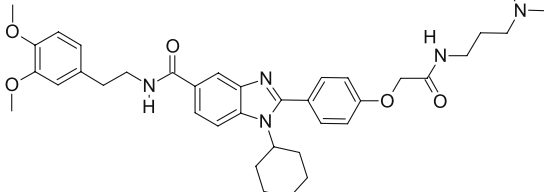
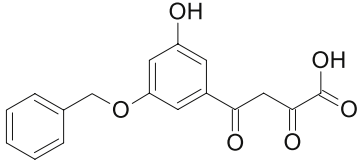
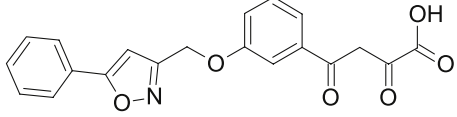
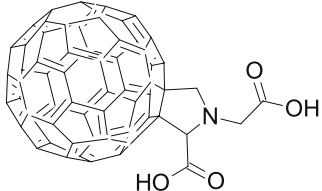
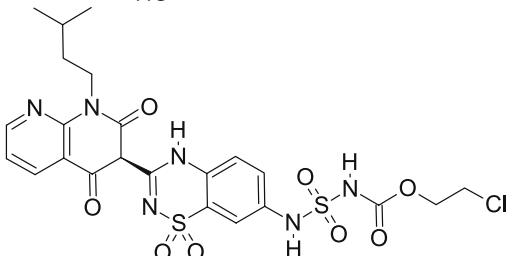
The best ranked 1% of the VS efforts for the BindingDB database HCV-NS5B inhibitors against the SARS CoV-2 RdRp (PDB ID: 7BV1). The ligand name and InChI key can be found in Table S3 in SM.

No.	Structure	Best score	Binding DB Monomer ID	Reference
		-91.84	50186172	[42]
		-91.33	50191537	[43]
		-90.49	50186142	[42]
		-90.44	50142043	[42]
		-89.71	50186161	[42]
		-89.59	50186160	[42]

(continued on next page)

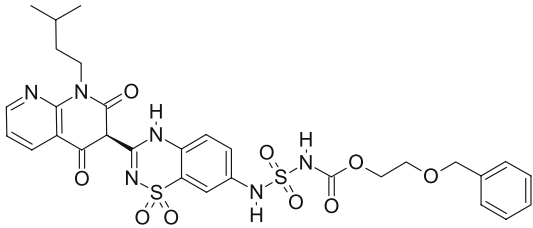
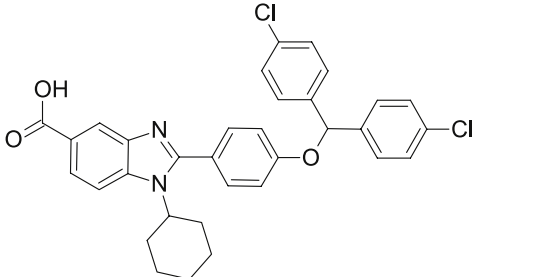
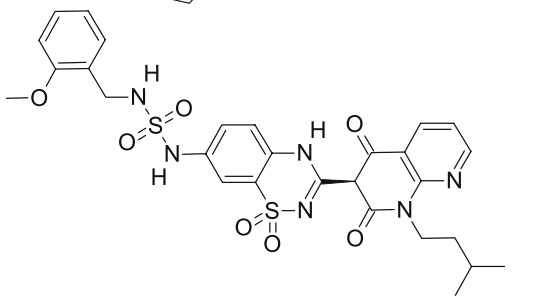
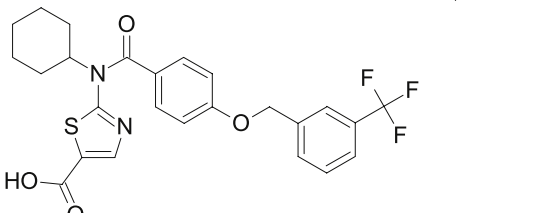
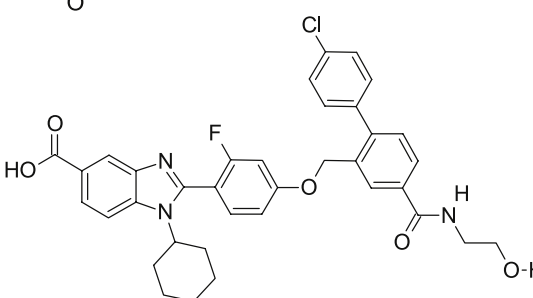
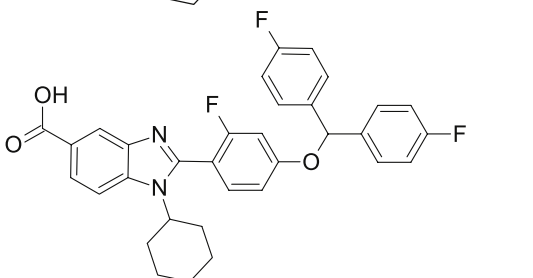


Table 2 (continued)

No.	Structure	Best score	Binding DB Monomer ID	Reference
		-89.43	50186165	[42]
		-88.65	50186141	[42]
		-88.50	50137476	[44]
		-88.35	50174478	[45]
		-87.99	50174454	[45]
		-87.88	50160864	[46]
		-87.83	50186148	[42]

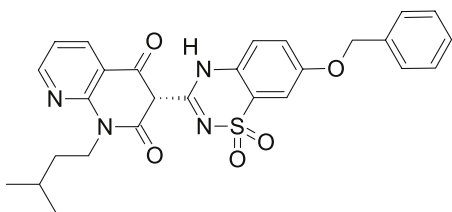
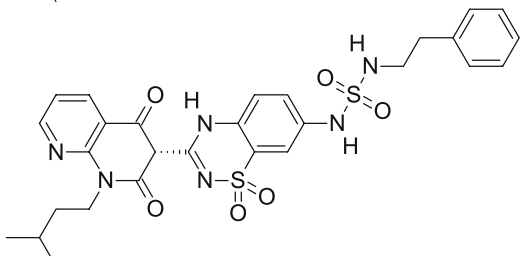
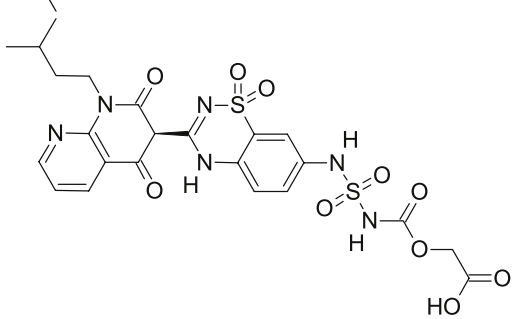
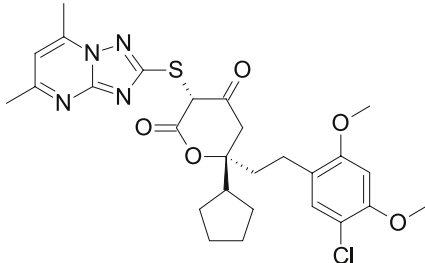
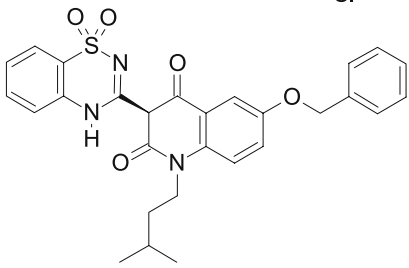
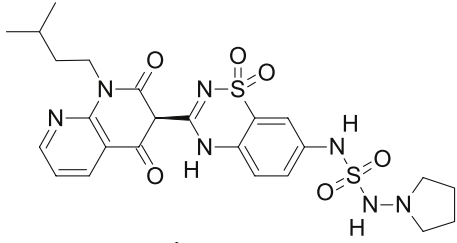
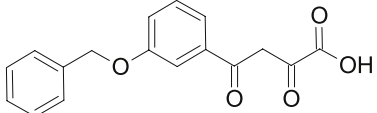
(continued on next page)

Table 2 (continued)

No.	Structure	Best score	Binding DB Monomer ID	Reference
		-87.13	50186163	[42]
		-86.66	50181932	[43]
		-86.59	50222336	[42]
		-86.23	50157198	[47]
		-86.03	50191548	[43]
		-85.53	50181927	[43]

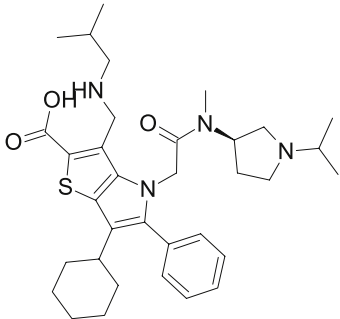
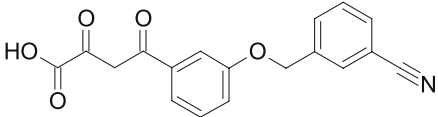
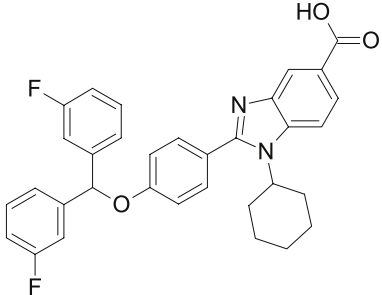
(continued on next page)

Table 2 (continued)

No.	Structure	Best score	Binding DB Monomer ID	Reference
		-85.52	50186208	[48]
		-85.49	50186139	[42]
		-85.47	50186143	[42]
		-85.45	50197038	[49]
		-85.27	50181668	[50]
		-85.04	50186159	[42]
		-84.82	50115572	[51]

(continued on next page)

Table 2 (continued)

No.	Structure	Best score	Binding DB Monomer ID	Reference
		-84.82	50081636	[52]
		-84.54	50137868	[51]
		-84.53	50181922	[43]

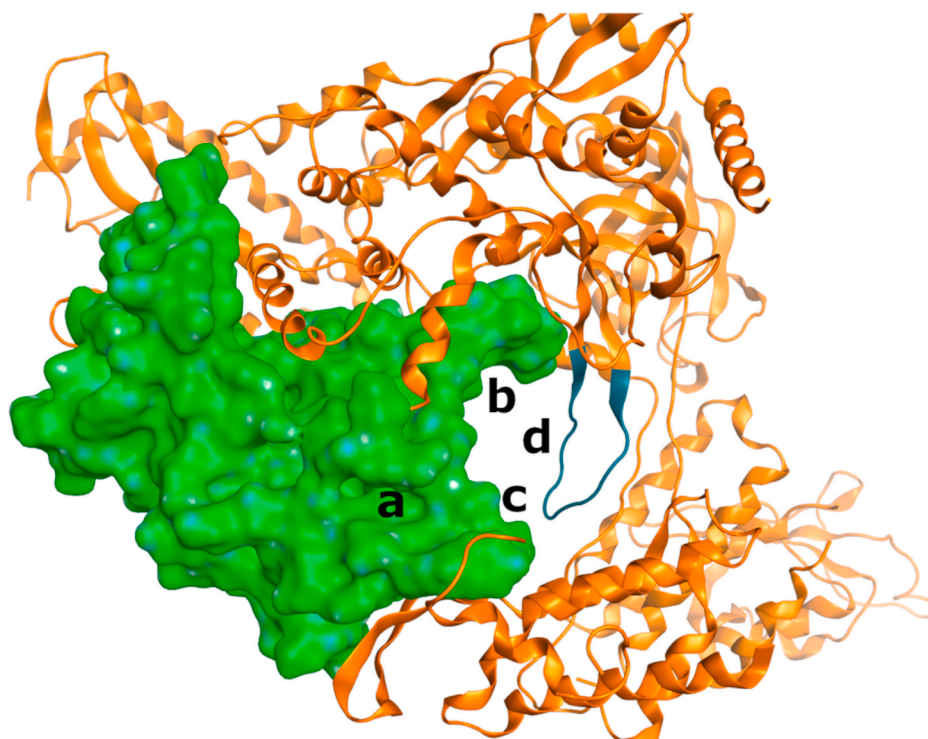
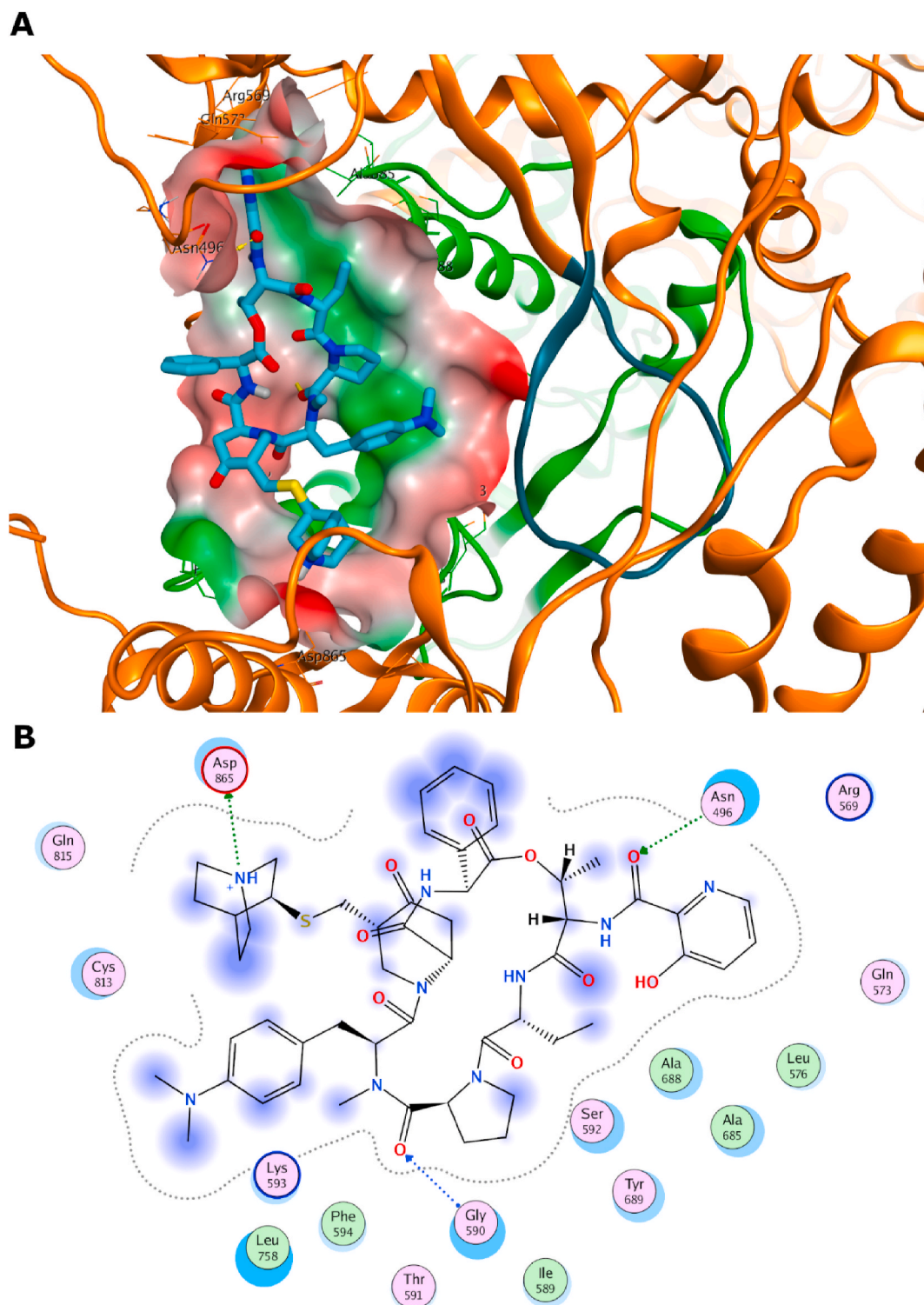


Fig. 5. The binding pockets occupied by the best ranked 1% of the VS efforts against SARS CoV-2 RdRp palm subdomain (PDB ID: 7BV1). The palm subdomain of RdRp is represented by a green surface and the grayish blue part of the ribbon refers to the F-motif. Ligands from the virtual screening efforts are occupying one of the four sites, a, b, c or d.

3HHK). Three highly cited docking tools, FRED, PLANTS and AutoDock Vina, were benchmarked against HCV NS5B palm subdomain. The benchmarking outcome suggested that PLANTS is the best performing

docking tool. The chemotype analysis via pROC-Chemotype plot for PLANTS showed that it can retrieve potent palm binders at the early enrichment. Based on the high similarity between HCV NS5B and SARS





**Fig. 6.** Docking pose of Quinupristin (DrugBank - cyan sticks) in the palm pocket of SARS CoV-2 polymerase (PDB ID: 7BV1), as 3D and 2D representations as (A) and (B), respectively. The hydrophilic and hydrophobic regions are in red and green colored molecular surfaces, respectively. The green ribbon part refers to the palm subdomain. The grayish blue part is for the F-motif. Dashed lines indicate favorable interactions. Non-polar hydrogens are omitted for clarification.

CoV2 RdRp, it is expected that PLANTS would show promising VS performance against the SARS CoV 2. Accordingly, PLANTS was selected to perform prospective virtual screening using both FDA-approved drugs (from DrugBank) and HCV NS5B-1b palm inhibitors (from BindingDB) against SARS CoV-2 RdRp (PDB ID: 7BV1). Inspection of the VS results recommended quinpristin, acetyldigitoxin and diosmin (from DrugBank) and compounds 1–3 (from BindingDB) to be potential binders to

SARS CoV-2 RdRp palm subdomain. Further stability evaluations by molecular dynamics simulations for 50 ns endorsed diosmin (from DrugBank) and compound 3 (from BindingDB) to be best potential binders to SARS CoV-2 RdRp palm subdomain.

This study displays a clear example of how to implement a DEKOIS 2.0 benchmark set against a crucial SARS CoV-2 target. This aids in enhancing the success rate of VS campaigns against SARS CoV-2

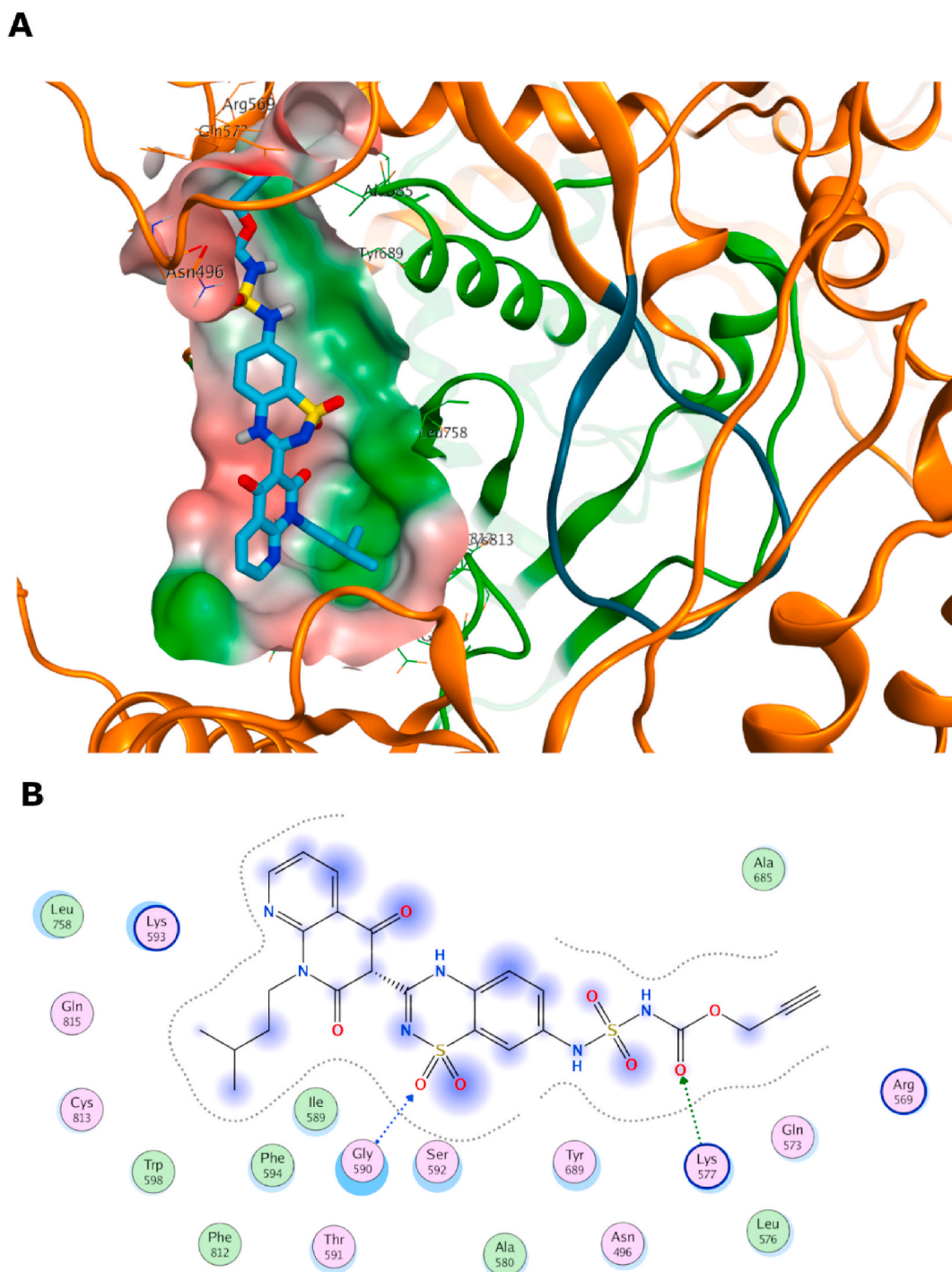


**Fig. 7.** Docking pose of compound number 2 (BindingDB) in the palm pocket of SARS CoV-2 polymerase (PDB ID: 7BV1) as 3D and 2D representations as (A) and (B), respectively. The color scheme is same as Fig. 6.

resolved targets. The identified top ranked, compounds from DrugBank and BindingDB databases are recommended to be subjected for further in vitro and in vivo investigations and repurposing against COVID-19.

#### 4. Methods

##### 4.1. Preparation of protein macromolecules

Molecular Operating Environment (MOE) [54], Chemical Computing Group Inc.: Montreal, <http://www.chemcomp.com>, was employed prior to the docking experiments to prepare the protein structures,

including: (i) HCV-NS5B structures (PDB ID: 3HHK), (ii) the SARS-CoV-2 RdRp (PDB ID: 7BV1). After eliminating the unessential ions, redundant chains, molecules of crystallization and unessential solvent molecules (if any), “Quickprep” Function of MOE was applied at default settings. Such parameters incorporate using “Protonate 3D” function to enhance H-bonding network and permit ASN/GLN/HIS to flip for optimum protonation and H-bonding networking. Additionally, the ligand and binding site atoms were refined through minimizing the energy to an RMS gradient of 0.1 kcal/mol/Å, while a force constant (strength = 10) was applied for the restraints of the binding site atoms. The remaining receptor atoms, which lie outside the binding pocket were kept the

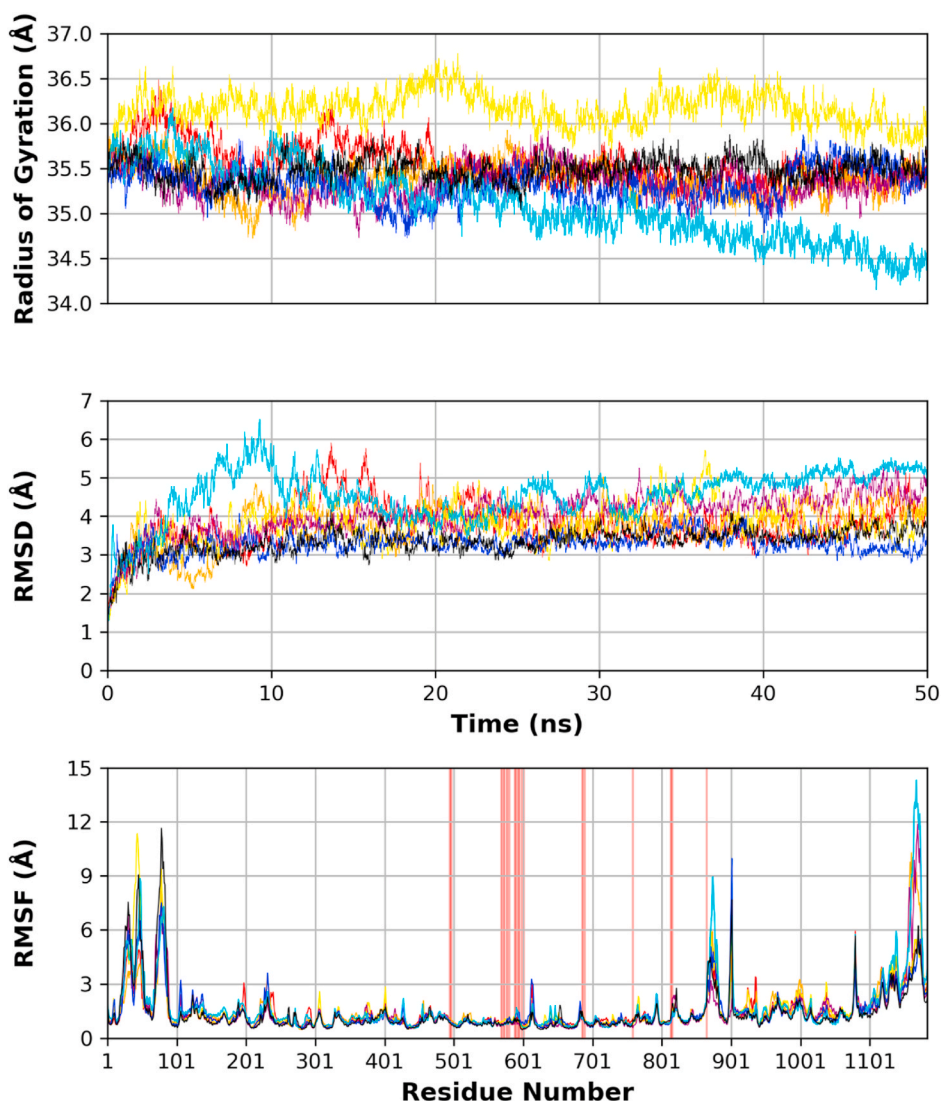


**Fig. 8.** Top: Radius of gyration (rgyr) of the protein during the simulation time. Middle: root mean square deviation (RMSD) of the protein alpha carbons during the simulation. Bottom: per residue root mean square fluctuation (RMSF). (red: compound 1, orange: compound 2, yellow: compound 3, purple: quinupristin, blue: acetyldigitoxin, cyan: diosmin, black: apo protein). The binding site amino acid residues are shown with red background.

same. The outcome of these parameters showed no significant difference concerning the binding site/ligand coordinates [55]. We conducted the benchmarking experiment on HCV-NS5B twice, including and excluding key water molecules in the palm subdomain, while the SARS-CoV-2 RdRp protein structure was used for the VS of DrugBank and HCV-NS5B palm inhibitors of BindingDB repository.

All protein superpositions were conducted using MOE.

#### 4.2. Preparation of small molecules including: DEKOIS 2.0 benchmark set, DrugBank database and BindingDB ligands

DEKOIS 2.0 [33] protocol was applied on 40 HCV-NS5B (genotype 1b) bioactives, which were extracted from BindingDB [19] and literature [18], to produce 1200 challenging decoys (1:30 ratio). All small molecules were prepared by MOE. ‘Molecule wash’ module was employed to create reliable protonation states via strong bases protonation and strong acids deprotonation (if required). The energy of the compounds was minimized using the Amber: 10EHT force field at a gradient of 0.01 RMSD. The rest options were kept at default settings. For each compound, one conformer was saved, and one protonation state was produced at pH 7.0. The stereo configuration of all molecules [19] was reserved [55]. The prepared compounds were kept as SD files

and used for FRED docking experiments. For docking experiments using AutoDock Vina, the SD files were transformed and split into individual PDBQT files by OpenBabel [56]. For PLANTS docking, the SDF files were converted into mol2 format and the correct atom types were set via SPORES software [57,58].

#### 4.3. Docking experiments

##### 4.3.1. For benchmarking

For docking using AutoDock Vina (version 1.1.2) [59], Python script (*prepare\_receptor4.py*) provided by the MGLTools package (version 1.5.4) was employed to convert protein files to PDBQT format [60]. The search algorithm efficiency was retained at a default level. However, to consider all the possible conformations of the docked molecules, the grid box docking dimensions were  $28 \text{ \AA} \times 28 \text{ \AA} \times 28 \text{ \AA}$ , with a spacing of 1 Å.

For docking using PLANTS [61], ‘ChemPLP’ was employed as the scoring function, with the ‘screen’ mode selected. The binding site was set to include the receptor atoms around the coordinates of the co-crystal ligand by 5 Å, in the palm subdomain of HCV-NS5B (PDB ID: 3HHK).

FRED docking [62,63] was set at default levels. OMEGA [64,65]. was used for generating different conformations of the ligands, actives and decoys. MakeReceptor GUI of OpenEye was utilized to describe the



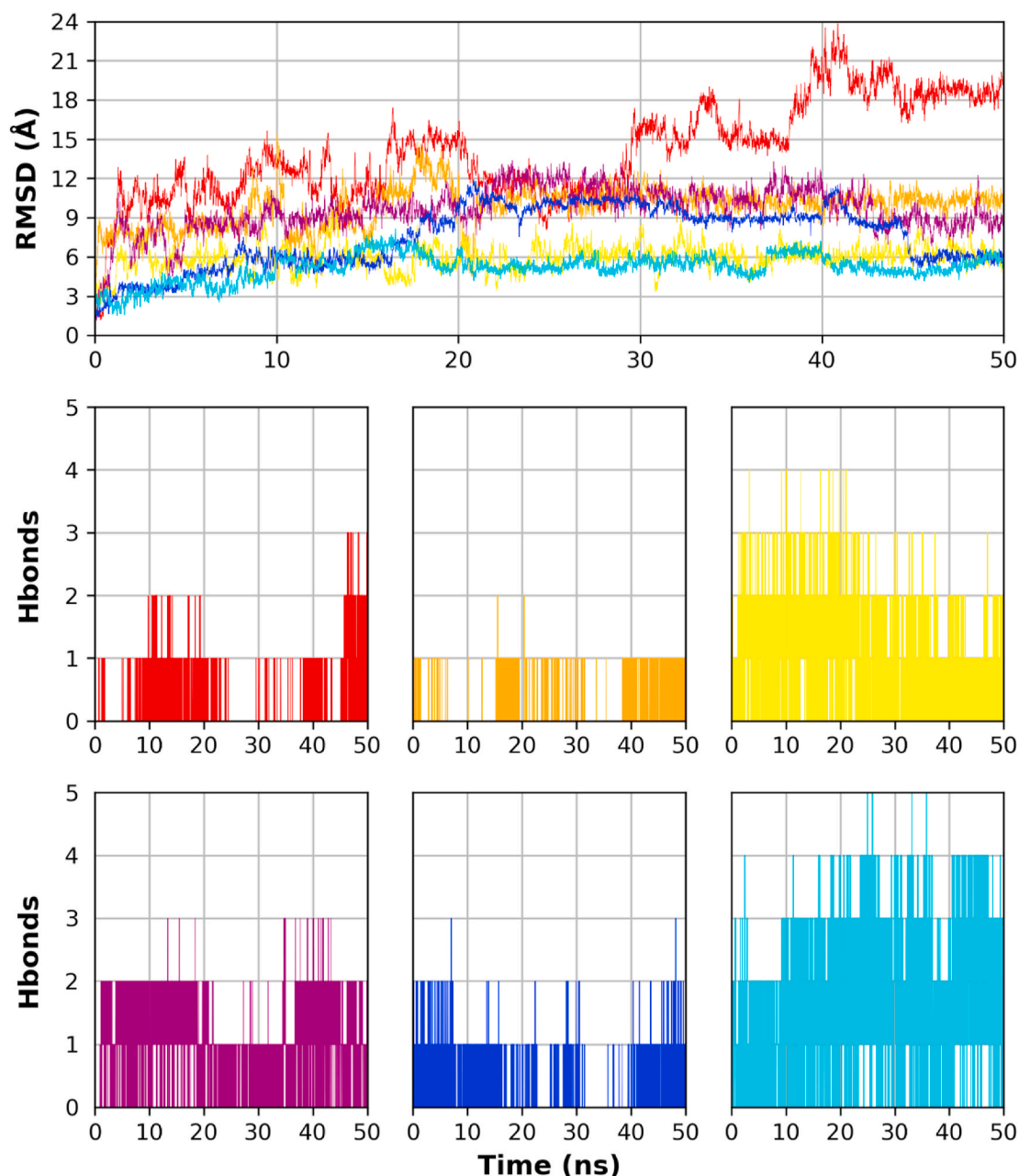


**Fig. 9.** Ligand RMSD and hydrogen bond analysis. (red: compound 1, orange: compound 2, yellow: compound 3, purple: quinupristin, blue: acetyldigitoxin, cyan: diosmin, black: apo protein).

binding pocket as a search box in the vicinity of the co-crystal ligand with dimensions of  $28.21 \text{ \AA} \times 28 \text{ \AA} \times 28.01 \text{ \AA}$ . Three water molecules were marked as a part of the protein since they are essential for mediating certain interactions between the protein amino acid residues and the ligand.

#### 4.3.2. For virtual screening of DrugBank and BindingDB ligands

Based on the superior performance of PLANTS in the benchmarking study, we selected it for virtual screening efforts against the SARS CoV-2 RdRp (PDB ID: 7BV1). The protein is an apo form and no PDB structure is available yet for a co-crystallized complex in the palm subdomain. Therefore, the palm binding site was defined via docking the co-crystal ligand of HCV-NS5B (PDB ID: 3HHK) into the palm subdomain of the apo structure of SARS CoV-2 RdRp (PDB ID: 7BV1). Then the docking search volume was defined based on  $5 \text{ \AA}$  around of the coordinates of the docked molecule.

#### 4.4. pROC and pROC-Chemotype calculations

The score-based docking order was utilized in calculating the pROC-AUC using “R-Snippet” component of KNIME [66], based on the subsequent equation [67].

$$pROCAUC = \frac{1}{n} \sum_i^n [-\log_{10}(D_i)] = \frac{1}{n} \sum_i^n \log_{10} \left( \frac{1}{D_i} \right)$$

The bioactives number is given by  $n$ , while  $D_i$  is the decoys fraction that is ordered higher than  $i$ th bioactive detected. Where  $i$ th is the number of the bioactive in the rank.

The pROC-Chemotype plots were created by the “pROC-Chemotype plot” tool accessible in <http://www.dekois.com/>, [36,37].

To assess the ability of the docking tool to recognize true positives, from the active set, in the score-ordered list compared to the random collection, enrichment factor (EF) was computed based on the following



equation [68].:

$$EF = \frac{Bioactives_{subset}}{N_{subset}} \bigg/ \frac{Bioactives_{total}}{N_{total}}$$

Chemical structures were drawn using ACD/ChemSketch Freeware (<https://www.acdlabs.com/resources/freeware/chemsketch/>).

#### 4.5. Molecular dynamics simulations

The molecular dynamics simulations were carried out as reported in this work [69]. Molecular dynamics simulations and systems build up were carried out using GROMACS 2020.3 [70]. Each protein-ligand complex was solvated in a dodecahedron box of TIP3P explicit water model [71]. System was then neutralized by NaCl molecules at 0.1 M concentration. Steepest descent minimization algorithm was used for system energy minimization setting 10 kJ/mol and 50,000 steps as convergence criteria. NVT followed by NPT equilibration were performed for 500 ps each at 300 K temperature and 1 atm pressure. Then, a production run was carried out for 50 ns at NPT ensemble. The V-rescale modified Berendsen thermostat [72] was used for temperature coupling for each equilibration run, while Berendsen coupling [73] was used for pressure coupling with 2 ps time constant for equilibration and production runs. On the other hand, Parrinello-Rahman pressure coupling scheme [74] was used for pressure coupling for the production runs. A Verlet cutoff-scheme was used for searching neighboring atoms and Van Der Waals calculations with cutoff and switch list distances of 1.2 and 1.0 nm, respectively. Particle Mesh Ewald method [75] was used for the calculations long-range electrostatics within 1.2 nm. Bond lengths were constrained using the LINear Constraint Solver (LINCS) algorithm [76]. CHARMM36 all-atom force field [77] was used for topology and parameter generation of the protein molecules, and SwissParam server [78] was used for ligand parameterization. For all simulations, a leap-frog integrator was used with a steps size of 2 fs. Protein RMSD, RMSF and radius of gyration was calculated out using ProDy python library [79,80], while ligand RMSD and hydrogen bonds were calculated using VMD rmsd trajectory analysis tool [81]. All analysis charts were constructed using Matplotlib python plotting library [82].

#### Conflicts of interest

All co-authors have seen and agree with the contents of the manuscript and there is no conflict of interest to report. We certify that the submission is original work and has not been published before and it is not under consideration for publication anywhere else.

#### CRedit authorship contribution statement

**Laila K. Elghoneimy:** Methodology, Visualization, Writing – original draft. **Muhammad I. Ismail:** Methodology, Visualization, Writing – review & editing. **Frank M. Boeckler:** Writing – review & editing. **Hassan M.E. Azzazy:** Supervision, Writing – review & editing. **Tamer M. Ibrahim:** Supervision, Conceptualization, Methodology, Visualization, Writing – review & editing.

#### Acknowledgments

The authors gratefully acknowledge the support of OpenEye Scientific Software Inc. for offering an academic license. Also, authors gratefully acknowledge the support of NVIDIA Corporation with the donation of the Titan Xp GPU used for molecular dynamics simulations. Authors thank Dr. Mahmoud S. Ahmed for offering simulation time on the GPU and Dr. Amgad Albohy for fruitful discussions about GROMACS MD simulations. TMI acknowledged the cluster of Bibliotheca Alexandrina High-Performance Computing for granting access to perform some of the molecular dynamics simulations. TMI thanks Matthias R. Bauer

(AstraZeneca, Cambridge, United Kingdom) for the fruitful discussions about DEKOIS 2.0 protocol.

#### Appendix A. Supplementary data

Supplementary data to this article can be found online at <https://doi.org/10.1016/j.compbiomed.2021.104468>.

#### Abbreviations

WHO	World Health Organization
COVID-19	corona virus disease 19
SARS-CoV-2	severe acute respiratory syndrome coronavirus 2
Nsp12	non-structural protein 12
NS5B	non-structural protein 5b
DEKOIS	Demanding Evaluation Kits for Objective In silico Screening
SBVS	structure based virtual screening.

#### References

- [1] D. Yang, J.L. Leibowitz, The structure and functions of coronavirus genomic 3' and 5' ends, *Virus Res.* 206 (2015) 120–133.
- [2] Y.A. Malik, Properties of coronavirus and SARS-CoV-2, *Malays. J. Pathol.* 42 (2020) 3–11.
- [3] L. Buonaguro, M. Tagliamonte, M.L. Tornesello, F.M. Buonaguro, SARS-CoV-2 RNA polymerase as target for antiviral therapy, *J. Transl. Med.* 18 (2020) 185.
- [4] Q. Wang, J. Wu, H. Wang, Y. Gao, Q. Liu, A. Mu, W. Ji, L. Yan, Y. Zhu, C. Zhu, X. Fang, X. Yang, Y. Huang, H. Gao, F. Liu, J. Ge, Q. Sun, X. Yang, W. Xu, Z. Liu, H. Yang, Z. Lou, B. Jiang, L.W. Guddat, P. Gong, Z. Rao, Structural basis for RNA replication by the SARS-CoV-2 polymerase, *Cell* 182 (2020) 417–428, e413.
- [5] Z. Zhao, P.E. Bourne, Structural insights into the binding modes of viral RNA-dependent RNA polymerases using a function-site interaction fingerprint method for RNA virus drug discovery, *J. Proteome Res.* 19 (2020) 4698–4705.
- [6] Y. Gao, L. Yan, Y. Huang, F. Liu, Y. Zhao, L. Cao, T. Wang, Q. Sun, Z. Ming, L. Zhang, J. Ge, L. Zheng, Y. Zhang, H. Wang, Y. Zhu, C. Zhu, T. Hu, T. Hua, B. Zhang, X. Yang, J. Li, H. Yang, Z. Liu, W. Xu, L.W. Guddat, Q. Wang, Z. Lou, Z. Rao, Structure of the RNA-dependent RNA polymerase from COVID-19 virus, *Science (New York, N.Y.)* 368 (2020) 779–782.
- [7] W. Yin, C. Mao, X. Luan, D.D. Shen, Q. Shen, H. Su, X. Wang, F. Zhou, W. Zhao, M. Gao, S. Chang, Y.C. Xie, G. Tian, H.W. Jiang, S.C. Tao, J. Shen, Y. Jiang, H. Jiang, Y. Xu, S. Zhang, Y. Zhang, H.E. Xu, Structural basis for inhibition of the RNA-dependent RNA polymerase from SARS-CoV-2 by remdesivir, *Science (New York, N.Y.)* 368 (2020) 1499–1504.
- [8] Y. Jiang, W. Yin, H.E. Xu, RNA-dependent RNA Polymerase: Structure, Mechanism, and Drug Discovery for COVID-19, *Biochemical and Biophysical Research Communications*, 2020.
- [9] F. Wu, S. Zhao, B. Yu, Y.M. Chen, W. Wang, Z.G. Song, Y. Hu, Z.W. Tao, J.H. Tian, Y.Y. Pei, M.L. Yuan, Y.L. Zhang, F.H. Dai, Y. Liu, Q.M. Wang, J.J. Zheng, L. Xu, E. C. Holmes, Y.Z. Zhang, A new coronavirus associated with human respiratory disease in China, *Nature* 579 (2020) 265–269.
- [10] L. Subissi, C.C. Posthuma, A. Collet, J.C. Zevenhoven-Dobbe, A.E. Gorbalenya, E. Decroly, E.J. Snijder, B. Canard, I. Imbert, One severe acute respiratory syndrome coronavirus protein complex integrates processive RNA polymerase and exonuclease activities, *Proc. Natl. Acad. Sci. U.S.A.* 111 (2014) E3900–E3909.
- [11] R.N. Kirchdoerfer, A.B. Ward, Structure of the SARS-CoV nsp12 polymerase bound to nsp7 and nsp8 co-factors, *Nat. Commun.* 10 (2019) 2342.
- [12] G. Schneider, Virtual screening: an endless staircase? *Nat. Rev. Drug Discov.* 9 (2010) 273–276.
- [13] T. Scior, A. Bender, G. Tresadern, J.L. Medina-Franco, K. Martínez-Mayorga, T. Langer, K. Cuanalo-Contreras, D.K. Agrafiotis, Recognizing pitfalls in virtual screening: a critical review, *J. Chem. Inf. Model.* 52 (2012) 867–881.
- [14] M. Schapira, R. Abagyan, M. Totrov, Nuclear hormone receptor targeted virtual screening, *J. Med. Chem.* 46 (2003) 3045–3059.
- [15] D.N. Santiago, Y. Pevzner, A.A. Durand, M. Tran, R.R. Scheerer, K. Daniel, S.-S. Sung, H. Lee Woodcock, W.C. Guida, W.H. Brooks, Virtual target screening: validation using kinase inhibitors, *J. Chem. Inf. Model.* 52 (2012) 2192–2203.
- [16] M.R. Bauer, T.M. Ibrahim, S.M. Vogel, F.M. Boeckler, Evaluation and optimization of virtual screening workflows with DEKOIS 2.0—a public library of challenging docking benchmark sets, *J. Chem. Inf. Model.* 53 (2013) 1447–1462.
- [17] T.M. Ibrahim, M.R. Bauer, F.M. Boeckler, Applying DEKOIS 2.0 in structure-based virtual screening to probe the impact of preparation procedures and score normalization, *J. Cheminf.* 7 (2015) 21.
- [18] M.J. Sofia, W. Chang, P.A. Furman, R.T. Mosley, B.S. Ross, Nucleoside, nucleotide, and non-nucleoside inhibitors of hepatitis C virus NS5B RNA-dependent RNA-polymerase, *J. Med. Chem.* 55 (2012) 2481–2531.
- [19] T. Liu, Y. Lin, X. Wen, R.N. Jorissen, M.K. Gilson, BindingDB: a web-accessible database of experimentally determined protein-ligand binding affinities, *Nucleic Acids Res.* 35 (2007) D198–D201.
- [20] F. Ruebsam, Z. Sun, B.K. Ayida, S.E. Webber, Y. Zhou, Q. Zhao, C.R. Kissinger, R. E. Showalter, A.M. Shah, M. Tsan, R. Patel, L.A. Lebrun, R. Kamran, M.V. Sergeeva,

- D.M. Bartkowski, T.G. Nolan, D.A. Norris, L. Kirkovsky, Hexahydro-pyrrolo- and hexahydro-1H-pyrrolo[1,2-b]pyridazin-2-ones as potent inhibitors of HCV NS5B polymerase, *Bioorg. Med. Chem. Lett* 18 (2008) 5002–5005.
- [21] D.A. Ellis, J.K. Blazel, S.E. Webber, C.V. Tran, P.S. Dragovich, Z. Sun, F. Ruebsam, H.M. McGuire, A.X. Xiang, J. Zhao, L.S. Li, Y. Zhou, Q. Han, C.R. Kissinger, R. E. Showalter, M. Lardy, A.M. Shah, M. Tsan, R. Patel, L.A. LeBrun, R. Kamran, D. M. Bartkowski, T.G. Nolan, D.A. Norris, M.V. Sergeeva, L. Kirkovsky, 4-(1,1-Dioxo-1,4-dihydro-1λ<sup>6</sup>-benzo[1,4]thiazin-3-yl)-5-hydroxy-2H-pyridazin-3-ones as potent inhibitors of HCV NS5B polymerase, *Bioorg. Med. Chem. Lett* 18 (2008) 4628–4632.
- [22] S.H. Kim, M.T. Tran, F. Ruebsam, A.X. Xiang, B. Ayida, H. McGuire, D. Ellis, J. Blazel, C.V. Tran, D.E. Murphy, S.E. Webber, Y. Zhou, A.M. Shah, M. Tsan, R. E. Showalter, R. Patel, A. Gobbi, L.A. LeBrun, D.M. Bartkowski, T.G. Nolan, D. A. Norris, M.V. Sergeeva, L. Kirkovsky, Q. Zhao, Q. Han, C.R. Kissinger, Structure-based design, synthesis, and biological evaluation of 1,1-dioxoisothiazole and benzo[b]thiophene-1,1-dioxide derivatives as novel inhibitors of hepatitis C virus NS5B polymerase, *Bioorg. Med. Chem. Lett* 18 (2008) 4181–4185.
- [23] F. Ruebsam, C.V. Tran, L.S. Li, S.H. Kim, A.X. Xiang, Y. Zhou, J.K. Blazel, Z. Sun, P. S. Dragovich, J. Zhao, H.M. McGuire, D.E. Murphy, M.T. Tran, N. Stankovic, D. A. Ellis, A. Gobbi, R.E. Showalter, S.E. Webber, A.M. Shah, M. Tsan, R.A. Patel, L. A. LeBrun, H.J. Hou, R. Kamran, M.V. Sergeeva, D.M. Bartkowski, T.G. Nolan, D. A. Norris, L. Kirkovsky, 5,6-Dihydro-1H-pyridin-2-ones as potent inhibitors of HCV NS5B polymerase, *Bioorg. Med. Chem. Lett* 19 (2009) 451–458.
- [24] A. Gopalsamy, R. Chopra, K. Lim, G. Ciszewski, M. Shi, K.J. Curran, S.F. Sukits, K. Svenson, J. Bard, J.W. Ellingboe, A. Agarwal, G. Krishnamurthy, A.Y. Howe, M. Orłowski, B. Feld, J. O'Connell, T.S. Mansour, Discovery of proline sulfonamides as potent and selective hepatitis C virus NS5b polymerase inhibitors. Evidence for a new NS5b polymerase binding site, *J. Med. Chem.* 49 (2006) 3052–3055.
- [25] J.A. Pfefferkorn, M.L. Greene, R.A. Nugent, R.J. Gross, M.A. Mitchell, B.C. Finzel, M.S. Harris, P.A. Wells, J.A. Shelly, R.A. Anstadt, R.E. Kilkuskie, L.A. Kopta, F. J. Schwende, Inhibitors of HCV NS5B polymerase. Part 1: evaluation of the southern region of (2Z)-2-(benzoylamino)-3-(5-phenyl-2-furyl)acrylic acid, *Bioorg. Med. Chem. Lett* 15 (2005) 2481–2486.
- [26] M.J. Slater, E.M. Amphlett, D.M. Andrews, G. Bravi, G. Burton, A.G. Cheasty, J. A. Corfield, M.R. Ellis, R.H. Fenwick, S. Fernandes, R. Guidetti, D. Haigh, C. D. Hartley, P.D. Howes, D.L. Jackson, R.L. Jarvest, V.L. Lovegrove, K.J. Medhurst, N.R. Parry, H. Price, P. Shah, O.M. Singh, R. Stocker, P. Thommes, C. Wilkinson, A. Wonacott, Optimization of novel acyl pyrrolidine inhibitors of hepatitis C virus RNA-dependent RNA polymerase leading to a development candidate, *J. Med. Chem.* 50 (2007) 897–900.
- [27] C.C. Cheng, G.W. Shippy Jr., Z. Yang, N. Kawahata, C.A. Lesburg, J.S. Duca, J. Bandoveres, J.D. Bracken, C.K. Jiang, S. Agrawal, E. Ferrari, H.C. Huang, Inhibitors of hepatitis C virus polymerase: synthesis and characterization of novel 2-oxy-6-fluoro-N-((S)-1-hydroxy-3-phenylpropan-2-yl)-benzamides, *Bioorg. Med. Chem. Lett* 20 (2010) 2119–2124.
- [28] C.C. Cheng, X. Huang, G.W. Shippy Jr., Y.S. Wang, D.F. Wyss, K.A. Soucy, C. K. Jiang, S. Agrawal, E. Ferrari, Z. He, H.C. Huang, Pyridine carboxamides: potent palm site inhibitors of HCV NS5B polymerase, *ACS Med. Chem. Lett.* 1 (2010) 466–471.
- [29] T. Nittoli, K. Curran, S. Insaf, M. DiGrandi, M. Orłowski, R. Chopra, A. Agarwal, A. Y. Howe, A. Prasad, M.B. Floyd, B. Johnson, A. Sutherland, K. Wheless, B. Feld, J. O'Connell, T.S. Mansour, J. Bloom, Identification of anthranilic acid derivatives as a novel class of allosteric inhibitors of hepatitis C NS5B polymerase, *J. Med. Chem.* 50 (2007) 2108–2116.
- [30] D. McGowan, O. Nyanguile, M.D. Cummings, S. Vendeville, K. Vandeyck, W. Van den Broeck, C.W. Boutton, H. De Bondt, L. Quiryren, K. De Amssoms, J.F. Bonfanti, S. Last, K. Rombauts, A. Tahri, L. Hu, F. Delouvroy, K. Vermeiren, G. Vandercruyssen, L. Van der Helm, E. Cleiren, W. Mostmans, P. Lory, G. Pille, K. Van Emelen, G. Fanning, F. Pauwels, T.I. Lin, K. Simmen, P. Raboison, 1,5-Benzodiazepine inhibitors of HCV NS5B polymerase, *Bioorg. Med. Chem. Lett* 19 (2009) 2492–2496.
- [31] K. Vandeyck, M.D. Cummings, O. Nyanguile, C.W. Boutton, S. Vendeville, D. McGowan, B. Devogelaere, K. Amssoms, S. Last, K. Rombauts, A. Tahri, P. Lory, L. Hu, D.A. Beauchamp, K. Simmen, P. Raboison, Structure-based design of a benzodiazepine scaffold yields a potent allosteric inhibitor of hepatitis C NS5B RNA polymerase, *J. Med. Chem.* 52 (2009) 4099–4102.
- [32] A.Y. Howe, H. Cheng, S. Johann, S.K. Chunduru, D.C. Young, J. Bard, R. Chopra, G. Krishnamurthy, T. Mansour, J. O'Connell, Molecular mechanism of hepatitis C virus replicon variants with reduced susceptibility to a benzofuran inhibitor, HCV-796, *Antimicrobial agents and chemotherapy* 52 (2008) 3327–3338.
- [33] M.R. Bauer, T.M. Ibrahim, S.M. Vogel, F.M. Boeckler, Evaluation and optimization of virtual screening workflows with DEKOIS 2.0—a public library of challenging docking benchmark sets, *J. Chem. Inf. Model.* 53 (2013) 1447–1462.
- [34] S.M. Vogel, M.R. Bauer, F.M. Boeckler, DEKOIS: demanding evaluation kits for objective in silico screening—a versatile tool for benchmarking docking programs and scoring functions, *J. Chem. Inf. Model.* 51 (2011) 2650–2665.
- [35] F.M. Boeckler, M.R. Bauer, T.M. Ibrahim, S.M. Vogel, Use of DEKOIS 2.0 to gain insights for virtual screening, *J. Cheminf.* 6 (2014) O24.
- [36] T.M. Ibrahim, M.R. Bauer, F.M. Boeckler, Probing the impact of protein and ligand preparation procedures on chemotype enrichment in structure-based virtual screening using DEKOIS 2.0 benchmark sets, *J. Cheminf.* 6 (2014) p19.
- [37] T.M. Ibrahim, M.R. Bauer, A. Dorr, E. Veyisoglu, F.M. Boeckler, pROC-chemotype plots enhance the interpretability of benchmarking results in structure-based virtual screening, *J. Chem. Inf. Model.* 55 (2015) 2297–2307.
- [38] D.R. Allington, M.P. Rivey, Quinupristin/dalfopristin: a therapeutic review, *Clin. Therapeut.* 23 (2001) 24–44.
- [39] D.S. Hage, A. Sengupta, Characterisation of the binding of digitoxin and acetyl digitoxin to human serum albumin by high-performance affinity chromatography, *J. Chromatogr. B Biomed. Sci. Appl.* 724 (1999) 91–100.
- [40] L. Hnátek, [Therapeutic potential of micronized purified flavonoid fraction (MPFF) of diosmin and hesperidin in treatment chronic venous disorder], *Vnitr. Lek.* 61 (2015) 807–814.
- [41] Y.A. Heo, E.D. Deeks, Sofosbuvir/velpatasvir/voxilaprevir: a review in chronic hepatitis C, *Drugs* 78 (2018) 577–587.
- [42] A.C. Krueger, D.L. Madigan, W.W. Jiang, W.M. Kati, D. Liu, Y. Liu, C.J. Maring, S. Masse, K.F. McDaniel, T. Middleton, H. Mo, A. Molla, D. Montgomery, J.K. Pratt, T.W. Rockway, R. Zhang, D.J. Kempf, Inhibitors of HCV NS5B polymerase: synthesis and structure-activity relationships of N-alkyl-4-hydroxyquinolon-3-yl-benzothiadiazine sulfamides, *Bioorg. Med. Chem. Lett* 16 (2006) 3367–3370.
- [43] S. Hirashima, T. Suzuki, T. Ishida, S. Noji, S. Yata, I. Ando, M. Komatsu, S. Ikeda, H. Hashimoto, Benzimidazole derivatives bearing substituted biphenyls as hepatitis C virus NS5B RNA-dependent RNA polymerase inhibitors: structure-activity relationship studies and identification of a potent and highly selective inhibitor JTK-109, *J. Med. Chem.* 49 (2006) 4721–4736.
- [44] P.L. Beaulieu, M. Bös, Y. Bousquet, P. DeRoy, G. Fazal, J. Gauthier, J. Gillard, S. Goulet, G. McKecher, M.A. Poupart, S. Valois, G. Kukolj, Non-nucleoside inhibitors of the hepatitis C virus NS5B polymerase: discovery of benzimidazole 5-carboxylic amide derivatives with low-nanomolar potency, *Bioorg. Med. Chem. Lett* 14 (2004) 967–971.
- [45] R. Di Santo, M. Fermeiglia, M. Ferrone, M.S. Paneni, R. Costi, M. Artico, A. Roux, M. Gabriele, K.D. Tardif, A. Siddiqui, S. Pricl, Simple but highly effective three-dimensional chemical-feature-based pharmacophore model for diketo acid derivatives as hepatitis C virus RNA-dependent RNA polymerase inhibitors, *J. Med. Chem.* 48 (2005) 6304–6314.
- [46] T. Mashino, K. Shimotohno, N. Ikegami, D. Nishikawa, K. Okuda, K. Takahashi, S. Nakamura, M. Mochizuki, Human immunodeficiency virus reverse transcriptase inhibition and hepatitis C virus RNA-dependent RNA polymerase inhibition activities of fullerene derivatives, *Bioorg. Med. Chem. Lett* 15 (2005) 1107–1109.
- [47] G.W. Shippy Jr., Y. Deng, T. Wang, J. Popovici-Muller, P.J. Curran, K.E. Rosner, A. B. Cooper, V. Girijavallabhan, N. Butkiewicz, M. Cable, Aminothiazole inhibitors of HCV RNA polymerase, *Bioorg. Med. Chem. Lett* 15 (2005) 115–119.
- [48] T.W. Rockway, R. Zhang, D. Liu, D.A. Betebenner, K.F. McDaniel, J.K. Pratt, D. Beno, D. Montgomery, W.W. Jiang, S. Masse, W.M. Kati, T. Middleton, A. Molla, C.J. Maring, D.J. Kempf, Inhibitors of HCV NS5B polymerase: synthesis and structure-activity relationships of N-1-benzyl and N-1-[3-methylbutyl]-4-hydroxy-1,8-naphthyridin-3-yl benzothiadiazine analogs containing substituents on the aromatic ring, *Bioorg. Med. Chem. Lett* 16 (2006) 3833–3838.
- [49] W. Hao, K.J. Herlihy, N.J. Zhang, S.A. Fuhrman, C. Doan, A.K. Patick, R. Duggal, Development of a novel dicistronic reporter-selectable hepatitis C virus replicon suitable for high-throughput inhibitor screening, *Antimicrob. Agents Chemother.* 51 (2007) 95–102.
- [50] R. Tedesco, A.N. Shaw, R. Bamba, D. Chai, N.O. Concha, M.G. Darcy, D. Dhanak, D.M. Fitch, A. Gates, W.G. Gerhardt, D.L. Halegoua, C. Han, G.A. Hofmann, V. K. Johnston, A.C. Kaura, N. Liu, R.M. Keenan, J. Lin-Goerke, R.T. Sarisky, K. J. Wiggall, M.N. Zimmerman, K.J. Duffy, 3-(1,1-dioxo-2H-(1,2,4)-benzothiadiazin-3-yl)-4-hydroxy-2(1H)-quinolinones, potent inhibitors of hepatitis C virus RNA-dependent RNA polymerase, *J. Med. Chem.* 49 (2006) 971–983.
- [51] V. Summa, A. Petrocchi, P. Pace, V.G. Matassa, R. De Francesco, S. Altamura, L. Tomei, U. Koch, P. Neuner, Discovery of alpha,gamma-diketo acids as potent selective and reversible inhibitors of hepatitis C virus NS5b RNA-dependent RNA polymerase, *J. Med. Chem.* 47 (2004) 14–17.
- [52] F. Zhao, N. Liu, P. Zhan, X. Jiang, X. Liu, Discovery of HCV NS5B thumb site I inhibitors: core-refining from benzimidazole to indole scaffold, *Eur. J. Med. Chem.* 94 (2015) 218–228.
- [53] M. Arba, S.T. Wahyudi, D.J. Brunt, N. Paradis, C. Wu, Mechanistic insight on the remdesivir binding to RNA-Dependent RNA polymerase (RdRp) of SARS-cov-2, *Comput. Biol. Med.* 129 (2021) 104156.
- [54] **Molecular Operating Environment, Chemical computing group Inc.: montreal.** <http://www.chemcomp.com>, 2018.
- [55] T.M. Ibrahim, M.I. Ismail, M.R. Bauer, A.A. Bekhit, F.M. Boeckler, Supporting SARS-CoV-2 papain-like protease drug discovery: in silico methods and benchmarking, *Frontiers in chemistry* 8 (2020) 592289.
- [56] N.M. O'Boyle, M. Banck, C.A. James, C. Morley, T. Vandermeersch, G. R. Hutchison, Open Babel: an open chemical toolbox, *J. Cheminf.* 3 (2011) 33.
- [57] T. ten Brink, T.E. Exner, Influence of protonation, tautomeric, and stereoisomeric states on Protein–Ligand docking results, *J. Chem. Inf. Model.* 49 (2009) 1535–1546.
- [58] T. ten Brink, T.E. Exner, pK(a) based protonation states and microspecies for protein-ligand docking, *J. Comput. Aided Mol. Des.* 24 (2010) 935–942.
- [59] O. Trott, A.J. Olson, AutoDock Vina, Improving the speed and accuracy of docking with a new scoring function, efficient optimization, and multithreading, *J. Comput. Chem.* 31 (2010) 455–461.
- [60] M.F. Sanner, Python: a programming language for software integration and development, *J. Mol. Graph. Model.* 17 (1999) 57–61.
- [61] O. Korb, T. Stutzle, T.E. Exner, Empirical scoring functions for advanced protein-ligand docking with PLANTS, *J. Chem. Inf. Model.* 49 (2009) 84–96.
- [62] M. McGann, FRED pose prediction and virtual screening accuracy, *J. Chem. Inf. Model.* 51 (2011) 578–596.
- [63] M. McGann, FRED and HYBRID docking performance on standardized datasets, *J. Comput. Aided Mol. Des.* 26 (2012) 897–906.

- [64] P.C.D. Hawkins, A. Nicholls, Conformer generation with OMEGA: learning from the data set and the analysis of failures, *J. Chem. Inf. Model.* 52 (2012) 2919–2936.
- [65] P.C.D. Hawkins, A.G. Skillman, G.L. Warren, B.A. Ellingson, M.T. Stahl, Conformer generation with OMEGA: algorithm and validation using high quality structures from the protein databank and Cambridge structural database, *J. Chem. Inf. Model.* 50 (2010) 572–584.
- [66] M.R. Berthold, N. Cebon, F. Dill, T.R. Gabriel, T. Kötter, T. Meinl, P. Ohl, C. Sieb, K. Thiel, B. Wiswedel, KNIME: the Konstanz Information Miner, *Studies in Classification, Data Analysis, and Knowledge Organization (GfKL 2007)*, Springer-Verlag, Heidelberg-Berlin, 2007.
- [67] R.D. Clark, D.J. Webster-Clark, Managing bias in ROC curves, *J. Comput. Aided Mol. Des.* 22 (2008) 141–146.
- [68] B.Q. Wei, W.A. Baase, L.H. Weaver, B.W. Matthews, B.K. Shoichet, A model binding site for testing scoring functions in molecular docking, *J. Mol. Biol.* 322 (2002) 339–355.
- [69] M.A. Said, A. Albohy, M.A. Abdelrahman, H.S. Ibrahim, Importance of glutamine 189 flexibility in SARS-CoV-2 main protease: lesson learned from in silico virtual screening of ChEMBL database and molecular dynamics, *Eur. J. Pharmaceut. Sci.* 160 (2021) 105744.
- [70] M.J. Abraham, T. Murtola, R. Schulz, S. Páll, J.C. Smith, B. Hess, E. Lindahl, GROMACS: high performance molecular simulations through multi-level parallelism from laptops to supercomputers, *Software* 1–2 (2015) 19–25.
- [71] P. Mark, L. Nilsson, Structure and dynamics of the TIP3P, SPC, and SPC/E water models at 298 K, *J. Phys. Chem.* 105 (2001) 9954–9960.
- [72] G. Bussi, D. Donadio, M. Parrinello, Canonical sampling through velocity rescaling, *J. Chem. Phys.* 126 (2007), 014101.
- [73] H.J.C. Berendsen, J.P.M. Postma, W.F.v. Gunsteren, A. DiNola, J.R. Haak, Molecular dynamics with coupling to an external bath, *J. Chem. Phys.* 81 (1984) 3684–3690.
- [74] M. Parrinello, A. Rahman, Polymorphic transitions in single crystals: a new molecular dynamics method, *J. Appl. Phys.* 52 (1981) 7182–7190.
- [75] T. Darden, D. York, L. Pedersen, Particle mesh Ewald: an N-log(N) method for Ewald sums in large systems, *J. Chem. Phys.* 98 (1993) 10089–10092.
- [76] B. Hess, H. Bekker, H.J.C. Berendsen, J.G.E.M. Fraaije, LINC: a linear constraint solver for molecular simulations, *J. Comput. Chem.* 18 (1997) 1463–1472.
- [77] J. Huang, A.D. MacKerell Jr., CHARMM36 all-atom additive protein force field: validation based on comparison to NMR data, *J. Comput. Chem.* 34 (2013) 2135–2145.
- [78] V. Zoete, M.A. Cuendet, A. Grosdidier, O. Michielin, SwissParam: a fast force field generation tool for small organic molecules, *J. Comput. Chem.* 32 (2011) 2359–2368.
- [79] A. Bakan, L.M. Meireles, I. Bahar, ProDy: protein dynamics inferred from theory and experiments, *Bioinformatics* 27 (2011) 1575–1577.
- [80] A. Bakan, A. Dutta, W. Mao, Y. Liu, C. Chennubhotla, T.R. Lezon, I. Bahar, Evol and ProDy for bridging protein sequence evolution and structural dynamics, *Bioinformatics* 30 (2014) 2681–2683.
- [81] W. Humphrey, A. Dalke, K. Schulten, VMD: visual molecular dynamics, *J. Mol. Graph.* 14 (1996) 33–38.
- [82] J.D. Hunter, Matplotlib: a 2D graphics environment, *Comput. Sci. Eng.* 9 (2007) 90–95.